

Effect of cover depth and rebar diameter on shrinkage behavior of ultra-high-performance fiber-reinforced concrete slabs

Doo-Yeol Yoo^{1a}, Ki-Yeon Kwon^{2b}, Jun-Mo Yang^{3c} and Young-Soo Yoon^{*4}

¹Department of Architectural Engineering, Hanyang University, Seoul, Korea

²Structural Systems & Site Evaluation Department, Korea Institute of Nuclear Safety, Daejeon, Korea

³Steel Structure Research Group, POSCO, Incheon, Korea

⁴School of Civil, Environmental and Architectural Engineering, Korea University, Seoul, Korea

(Received January 9, 2015, Revised November 11, 2016, Accepted November 15, 2016)

Abstract. This study investigates the effects of reinforcing bar diameter and cover depth on the shrinkage behavior of restrained ultra-high-performance fiber-reinforced concrete (UHPFRC) slabs. For this, twelve large-sized UHPFRC slabs with three different rebar diameters ($d_b=9.5, 15.9, \text{ and } 22.2$ mm) and four different cover depths ($h=5, 10, 20, \text{ and } 30$ mm) were fabricated. In addition, a large-sized UHPFRC slab without steel rebar was fabricated for evaluating degree of restraint. Test results revealed that the uses of steel rebar with a large diameter, leading to a larger reinforcement ratio, and a low cover depth are unfavorable regarding the restrained shrinkage performance of UHPFRC slabs, since a larger rebar diameter and a lower cover depth result in a higher degree of restraint. The shrinkage strain near the exposed surface was high because of water evaporation. However, below a depth of 18 mm, the shrinkage strain was seldom influenced by the cover depth; this was because of the very dense microstructure of UHPFRC. Finally, owing to their superior tensile strength, all UHPFRC slabs with steel rebars tested in this study showed no shrinkage cracks until 30 days.

Keywords: ultra-high-performance fiber-reinforced concrete; slab; shrinkage; degree of restraint; steel rebar; cover depth; rebar diameter

1. Introduction

Ultra-high-performance fiber-reinforced concrete (UHPFRC), developed in many countries, shows superior mechanical strength (compressive strength is over 150 MPa and design tensile strength is 8 MPa), toughness, durability, and bond capacity (Richard and Cheyrezy 1995, AFGC 2013, Yoo *et al.* 2014a). Excellent performance can be achieved from UHPFRC by reducing its water-to-binder ratio (W/B) and by incorporating high-fineness admixtures in accordance with the packing density theory and a high volume of steel fibers (Richard and Cheyrezy 1995). In particular, owing to its strain-hardening response under tension and outstanding bond capacities, UHPFRC has become a very attractive material for fabricating thin-plate structures (i.e., slabs, thin walls, and roofs) and bridge deck joints (Kobler and Sobek 2008, Perry and Weiss 2009, Saleem *et al.* 2011, Kim *et al.* 2013).

However, due to its low W/B and the addition of high-

fineness admixtures, UHPFRC exhibits very high autogenous shrinkage (Yoo *et al.* 2014b). Kamen *et al.* (2007) reported that UHPFRC has fast kinetics of autogenous shrinkage (i.e., approximately 39% of the ultimate (one year) autogenous shrinkage was obtained at initial 7 days, given a 20°C curing). This was attributed to the fast hydration process, leading to the reduction of internal relative humidity and the microstructure evolution causing a modification of pore structures. If such high shrinkage of UHPFRC is restrained by external forms or internal reinforcing bar or contiguous members, high residual tensile stress will be generated in the concrete that will lead to shrinkage cracking. For this reason, the JSCE recommendation (JSCE 2004) mentioned that a deformed steel rebar should be carefully applied to UHPFRC structures because of the high possibility of shrinkage cracking. In particular, since thin-plate structures and bridge deck joints have very small cross-sectional areas and include reinforcing bars, these structures made of UHPFRC are highly vulnerable to cracking due to restraint of shrinkage. Thus, several studies (Habel *et al.* 2006, Park *et al.* 2013, Park *et al.* 2014, Yoo *et al.* 2014b, Yoo *et al.* 2014c) have been carried out to estimate the restrained shrinkage and cracking behavior of UHPFRC at material and structural levels. Most of these studies have been focused on investigating the shrinkage and cracking behavior of UHPFRC restrained by the external frame and form. To the best of our knowledge, only few studies (Yoo *et al.* 2014b, Yoo *et al.* 2015) have been published on the shrinkage behavior of UHPFRC restrained by internal

*Corresponding author, Professor

E-mail: ysyoon@korea.ac.kr

^aAssistant Professor

E-mail: dyoo@hanyang.ac.kr

^bSenior Researcher

E-mail: k729kky@kins.re.kr

^cSenior Researcher

E-mail: junrhkd@gmail.com

Table 1 Mix proportion

| Relative weight ratios to cement | | | | | | | | |
|----------------------------------|-------|-------------|------|--------------|------------------|------|-------|--------------------------|
| Cement | Water | Silica fume | Sand | Silica flour | Superplasticizer | SRA | EA | Steel fiber (V_f , %) |
| 1.00 | 0.25 | 0.25 | 1.10 | 0.30 | 0.016 | 0.01 | 0.075 | 2% |

[Note] V_f =fiber volume fraction, SRA=shrinkage-reducing admixture, EA=expansive admixture

reinforcing bars. However, since the main purpose of their previous research was to investigate the effects of the rebar type, reinforcement ratio, and amount of shrinkage-reducing admixture (SRA) on the restrained shrinkage behavior of UHPFRC, a restrained shrinkage test was performed using a single embedded reinforcing bar under sealed conditions, according to the recommendations of the technical committee on autogenous shrinkage at JCI (JCI 1999). Thus, the previous studies were limited to the simulation of the real shrinkage behavior of UHPFRC slabs or bridge deck joints restrained by internal reinforcing bars. Furthermore, owing to insufficient information about the shrinkage behavior of UHPFRC restrained by an internal rebar, the design of UHPFRC structures and their application as real structures have been very limited despite the various advantages of UHPFRC.

Accordingly, in this study, to investigate the shrinkage behavior of thin UHPFRC slabs restrained by internal reinforcing bars, twelve large-sized UHPFRC slabs with various rebar diameters and cover depths were fabricated and tested. In addition, to evaluate the degree of restraint-an important parameters affecting the restrained shrinkage performance of concrete-a same-sized UHPFRC slab without steel rebar was fabricated.

2. Experimental program

2.1 Material properties

Portland cement and silica fume (SF) were used as cementitious materials. The specific surface area of the cement and SF were 3413 and 200000 cm^2/g , respectively, and their densities were 3.15 and 2.10 g/cm^3 , respectively. The cement included CaO, SiO_2 , and Al_2O_3 values of 61.33, 21.01, and 6.40, respectively, and SF included CaO, SiO_2 , and Al_2O_3 values of 0.38, 96.00, and 0.25, respectively. Sand with a grain size smaller than 0.5 mm was used as a fine aggregate, and silica flour having a diameter of 2 μm and 98% SiO_2 was used as a filler. To achieve suitable fluidity, polycarboxylate superplasticizer (SP) with a density of 1.06 g/cm^3 was added to the mixture. Further, high strength steel fibers with a diameter of 0.2 mm and a length of 13 mm were incorporated in the mixture. The detailed properties of the used materials can be found in a previous research (Yoo *et al.* 2014a).

Owing to the effectiveness of the combined use of a SRA and an expansive admixture (EA) on the restrained shrinkage behavior of UHPFRC (Park *et al.* 2014), a mixture including 1% SRA and 7.5% EA has been used as the standard UHPFRC mixture in Korea. Approximately 50% of free shrinkage of UHPFRC was reduced by the

combined use of EA and SRA (Yoo *et al.* 2014c). This is attributed to the fact that the EA compensated the early age shrinkage strain by expansion, and the SRA decreased the surface tension of pore water in hardened cement paste, leading to a reduced capillary stress (Rajabipour *et al.* 2008). Moreover, some of the structures in Korea were built using UHPFRC with 1% SRA and 7.5% EA (Kim *et al.* 2013). Therefore, in this study, CSA EA with a specific surface area of 3117 cm^2/g and a density of 2.98 g/cm^3 , and glycol-based SRA named "METOLAT P 860", produced by Münzing Chemie GmbH in Germany, were incorporated in the concrete mixture.

2.2 Mix proportion and mixing sequence

The mix proportion investigated in this study is given according to the weight ratio in Table 1. A W/B value of 0.2 was used, and due to its low W/B, 1.6% SP was incorporated in the mixture by the weight of cement. In order to improve the tensile performance and to reduce shrinkage, 2% (by volume) of smooth steel fibers were incorporated in the mixture, which is very similar to the UHPFRC mixture commercially available in North America (Graybeal 2008). In addition, as mentioned previously, 1% SRA and 7.5% EA were included in the mixture to decrease shrinkage.

The mixing sequence for preparing UHPFRC is as follows: first, cement, SF, silica flour, and sand were dry-mixed for about 10 min. Thereafter, water premixed with SP was added and mixed for another 10 min. When the mortar matrix showed good fluidity and adequate viscosity, the steel fibers were added by hand and mixed for an additional 5 min for ensuring uniform fiber dispersion.

2.3 Test setup and procedure

2.3.1 Properties of fresh concrete

According to ASTM C 1437 (ASTM 2007), a flow table test was performed to measure the fluidity of the prepared UHPFRC. Fresh concrete was first placed on the flow table in a cone-shaped mold. The mold was lifted-off slowly, and then the flow table was dropped 25 times in 15 sec. The flow value of UHPFRC obtained by averaging the maximum flow diameter and perpendicular diameter was found to be 200 mm.

The setting properties of UHPFRC were investigated using a penetration resistance test in accordance with ASTM C 403 (ASTM 2008). Yoo *et al.* (2013) have reported that owing to the low W/B of UHPFRC, a 5-10-mm-thick layer of liquid paraffin oil should be applied on the top surface of mortar to prevent the undesirable effect of dry skin formation during the penetration resistance test.

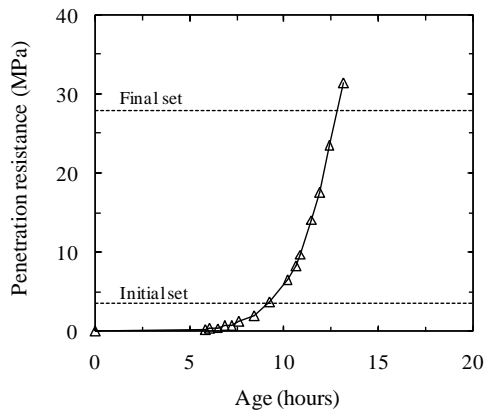


Fig. 1 Penetration resistance test results

Thus, ϕ 150×160 mm sized cylindrical plastic mold was used and mortar was filled up to a height of 150 mm with liquid paraffin oil applied on the mortar surface. A needle was penetrated into the mortar to a depth of 25 ± 2 mm in 10 sec with a clear distance rule of needle impression. Initial and final setting times were determined when the pressure obtained by the needle penetration reached to 3.5 N/mm^2 and 28 N/mm^2 , respectively. The times for initial and final sets obtained were 9.2 h and 12.8 h, respectively (see Fig. 1).

2.3.2 Shrinkage tests for UHPFRC slabs

To investigate the effects of cover depth and steel rebar diameter on the restrained shrinkage behavior of UHPFRC slabs, four different cover depths ($h=5, 10, 20,$ and 30 mm) and three different diameters ($d_b=9.5, 15.9,$ and 22.2 mm) of the upper rebar were considered. The main purpose of changing rebar diameter was to provide different steel-concrete ratios (or reinforcement ratios), and to investigate their effects on the restrained shrinkage behavior of UHPFRC. It was reported that the restrained shrinkage behavior of UHPFRC is influenced by the reinforcement ratio (Yoo *et al.* 2014b). Therefore, the number of steel rebar was fixed but diameter was changed, and it was assumed that the size effect of steel rebar on the restrained shrinkage of UHPFRC was negligible at the identical reinforcement ratio. The detailed properties of the steel rebar used in this study are summarized in Table 2. The shrinkage tests of UHPFRC slabs were performed using a $600 \times 600 \times 100$ mm sized prismatic specimen, as shown in Fig. 2(a). To induce the restraint effect of the contiguous element, the specimen side was restrained by studs. In addition, to eliminate the thermal deformation effect of the external frame on the shrinkage behavior of UHPFRC slabs, wood was adopted as an external form rather than steel. For obtaining identical boundary conditions, a steel rebar with $d_b=12.7$ mm was used as the bottom reinforcement in all test series. Two strain gages and one thermocouple were attached at the center of the upper steel rebar to measure the strain and temperature in steel rebar. Since the strain in steel is very sensitive to temperature variations, a dumbbell-shaped strain gage having nearly zero stiffness and a coefficient of thermal expansion of $11 \mu\epsilon/^\circ\text{C}$, similar to that of hardened concrete, was also installed adjacent to the

Table 2 Properties of deformed steel rebar

| Nominal diameter (mm) | Area (mm^2) | Elastic modulus (GPa) | Yield strength (MPa) | Ultimate strength (MPa) |
|-----------------------|------------------------|-----------------------|----------------------|-------------------------|
| $d_b=9.5\text{mm}$ | 71.3 | | 500.7 | 626.2 |
| $d_b=15.9\text{mm}$ | 198.6 | 200.0 | 488.4 | 607.1 |
| $d_b=22.2\text{mm}$ | 387.1 | | 506.3 | 615.7 |

[Note] d_b =nominal diameter of steel rebar

upper steel rebar for measuring the restrained shrinkage strain of UHPFRC.

In addition, to evaluate the degree of restraint according to internal steel rebar, a same sized prismatic specimen was fabricated without rebar. To take into account the restraint of the contiguous element, studs were also installed in the external frame. Six dumbbell-shaped strain gages and six thermocouples were installed for measuring the shrinkage strain and temperature of UHPFRC near the location of the steel rebar. These instruments were installed before concrete casting for immediately measuring the shrinkage strain after the start of casting, as shown in Fig. 2(b).

All specimens were tested in the normal atmosphere; the temperature and relative humidity during the testing are shown in Fig. 3. The average temperature and relative humidity were found to be 21.6°C (ranging from 17.4°C to 25.7°C) and 62.2% (ranging from 33.1% to 82.1%), respectively.

3. Results and discussion

3.1 Determination of zeroing point of shrinkage measurement

When concrete is fresh, no residual stress due to restraint of shrinkage occurs in concrete because of its nearly zero stiffness. To consider the shrinkage strain, which causes cracking in concrete, therefore, strain observed when the concrete is fresh was excluded. In addition, Aitcin (1999) reported that as the measurement of autogenous shrinkage starts after 24 h, as per ASTM C157 (ASTM 2008), a considerable part of initial autogenous shrinkage is missed. Thus, several researchers (JCI 1999, Jiang *et al.* 2014, Sant *et al.* 2011, Yoo *et al.* 2014b) have used various starting points of shrinkage measurement, such as initial set (JCI 1999, Jiang *et al.* 2014), final set (Sant *et al.* 2011), and starting point of residual stress in concrete development (Yoo *et al.* 2014b), in order to evaluate actual amount of shrinkage causing cracks in concrete structures. However, Chang-wen *et al.* (2007) insisted that the zeroing point of self-desiccation shrinkage determined by concrete's setting time (from penetration methods) is not reliable for both physical definition and practical testing. Therefore, the point where residual stress in concrete is first developed by restraint of shrinkage is determined to be considered as the zeroing point of shrinkage measurement, according to a previous study (Yoo *et al.* 2014b). This point is also known as close to the deviation point between the shrinkage strain and temperature.

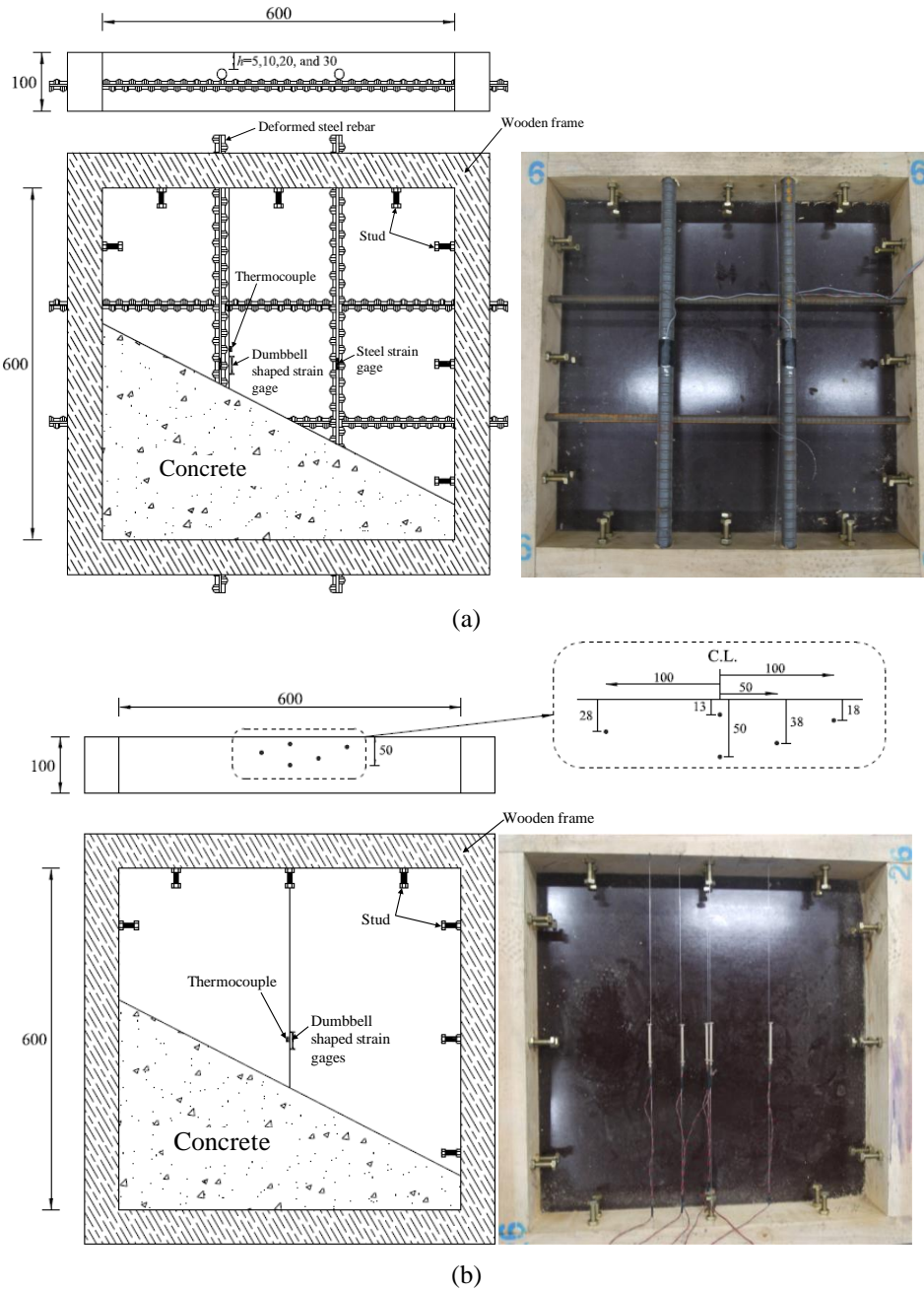


Fig. 2 Geometry and test setup for shrinkage tests of UHPFRC slabs (unit: mm); (a) slabs w/ steel rebars, (b) slab w/o rebar

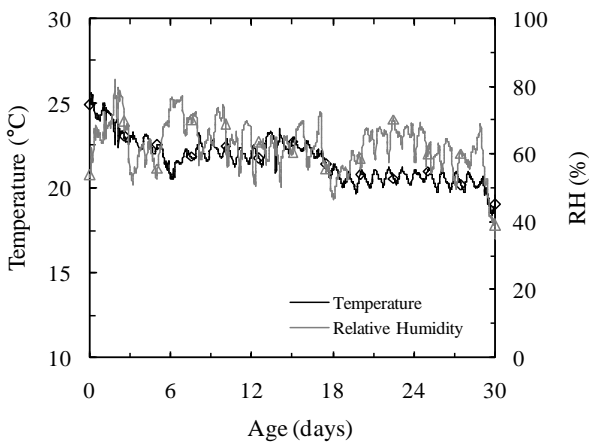


Fig. 3 Ambient temperature and relative humidity

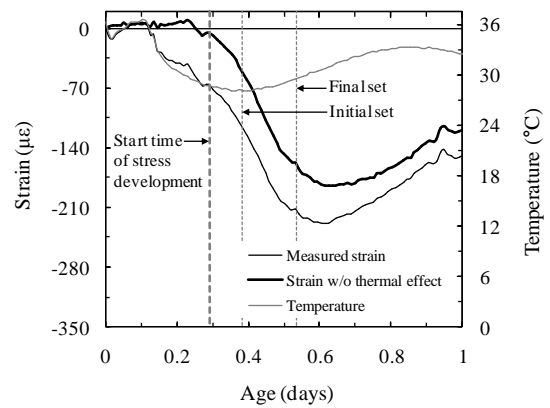


Fig. 4 Comparison of strain and temperature measured in steel rebar ($d_b=15.9$ mm)

Fig. 4 shows the early age strain and temperature in the steel rebar with a diameter of 15.9 mm. At a very early age, the steel rebar was deformed by temperature variation. The initial temperature of steel rebar was found to be 36.5 °C due to a high temperature of fresh concrete, while the ambient temperature at the same time was obtained as 24.9 °C. Since the temperature of steel rebar was higher than the ambient temperature, its temperature decreased to the ambient temperature, thereby resulting in volume contraction in the steel rebar and also the concrete. However, after nearly 7 h, compressive strain in the steel rebar steeply increased even though the rate of temperature decrease was reduced. Thus, the strain excluding thermal effect started to increase from this point, because the steel rebar was deformed by concrete shrinkage with hardening rather than the temperature gradient. Accordingly, this point was defined as the start time of stress development in the concrete due to restraint of shrinkage and was determined as the zeroing point of shrinkage measurement (called “time-zero” hereafter) to exclude the strain in the fresh concrete. The zeroing point was reached 2.2 h and 5.8 h faster than the initial and final sets, respectively.

3.2 Shrinkage behavior

Fig. 5 exhibits the initial strain and internal temperature behaviors of UHPFRC slab without steel rebar. Before time-zero, the measured strain increased in minus direction with decreasing internal concrete temperature. This measured strain is not a shrinkage of UHPFRC, but a volume change by temperature variation from a higher temperature of fresh concrete to a lower atmosphere temperature. On the other hand, after time-zero, the strain rapidly increased and showed different behavior to that of temperature, similar to the results reported in a previous study (Yoo *et al.* 2014b). The maximum internal temperature by hydration heat was found to be 33.3 °C, and after that, it was gradually reduced to the ambient temperature. Approximately 16 h after concrete casting, the specimen expanded due to this hydration heat of cement and EA addition.

The shrinkage and temperature of UHPFRC measured

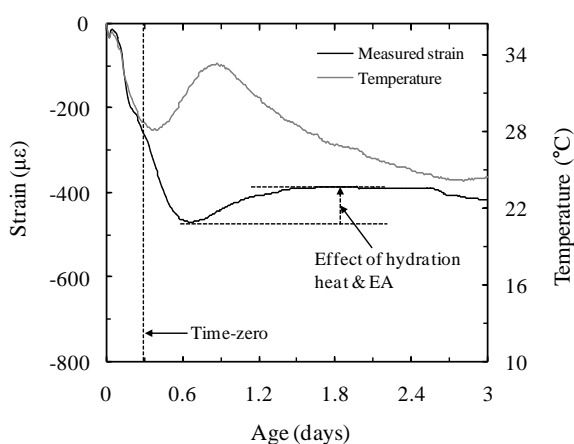


Fig. 5 Early age strain and temperature behaviors of UHPFRC slab without steel rebar at $h=13$ mm

from time-zero at different depths are shown in Fig. 6. The shrinkage strains increased very steeply with age until 16 h and then the specimen slightly expanded. After the slight expansion, the strains gradually reincreased and converged to a stable value. The highest shrinkage strain after 30 days was found to be $-605 \mu\epsilon$ ($\mu\epsilon = 10^{-6}$ m/m) at a depth of 13 mm (lowest depth). This is attributed to the fact that since water evaporation is most severe at near the exposed surface, the largest magnitude of shrinkage strain, caused by the evaporation of water, was obtained at the point with the lowest depth. Interestingly, the shrinkage strains obtained below $h = 18$ mm showed similar values, as shown in Fig. 7. This is because owing to the very dense microstructure of UHPFRC, the effect of water evaporation from the exposed surface on the shrinkage behavior became insignificant below 18 mm. However, temperature showed similar trends and values regardless of the distance from the top surface (Fig. 6(b)).

Fig. 8 exhibits a comparison between the restrained strains and the shrinkage strain in concrete without rebar. Herein, the restrained strains indicate the strains measured

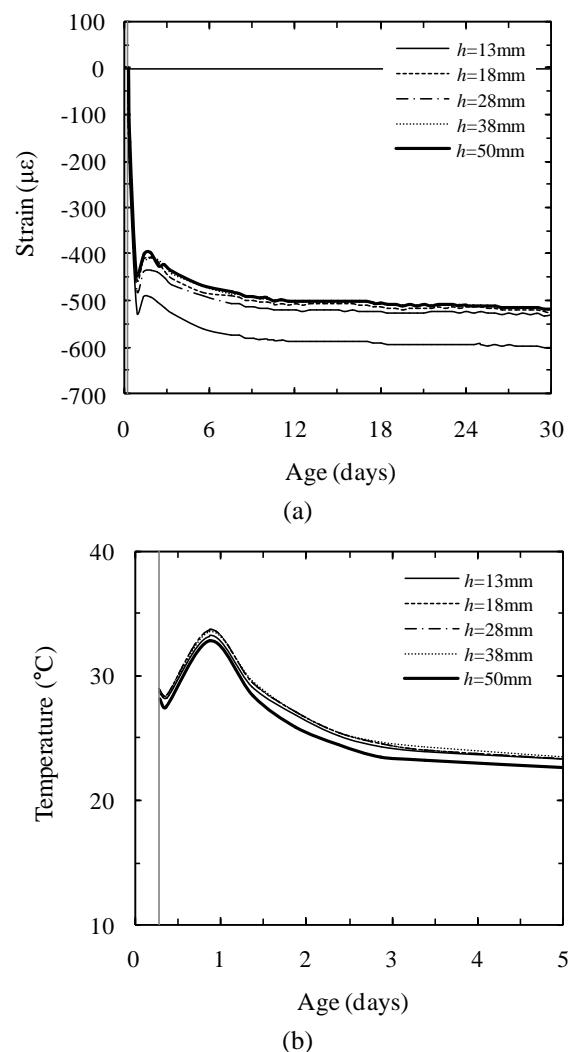


Fig. 6 Shrinkage and temperature behaviors of UHPFRC slab without rebar; (a) shrinkage strains at different depths, (b) temperature gradients at different depths

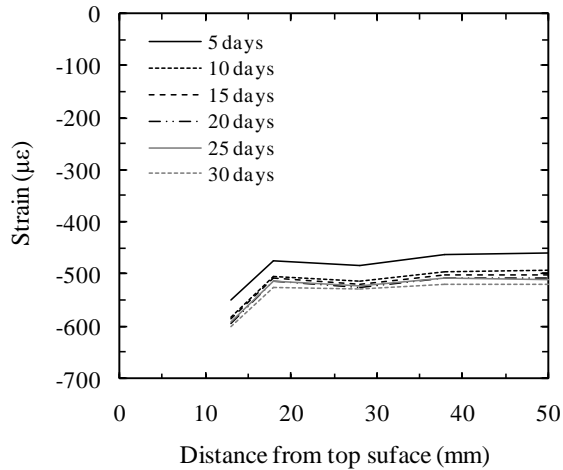


Fig. 7 Shrinkage according to distance from top surface

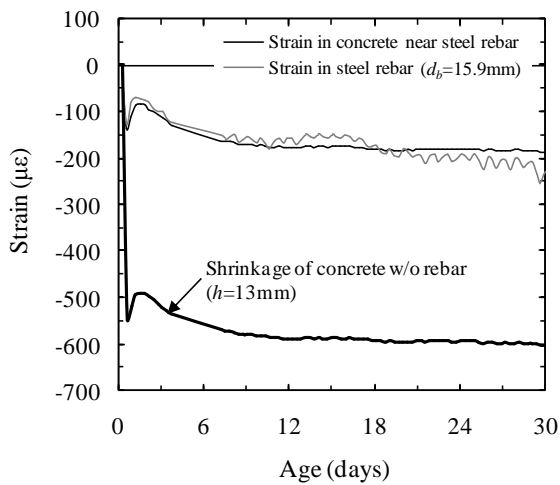
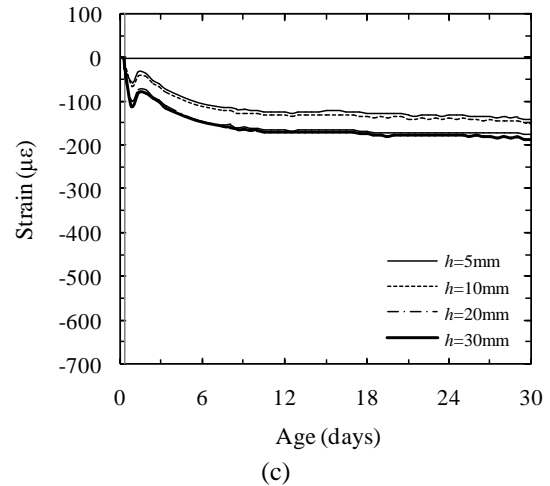
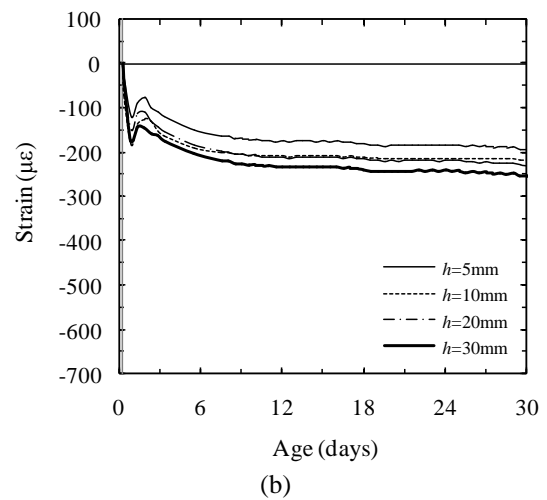
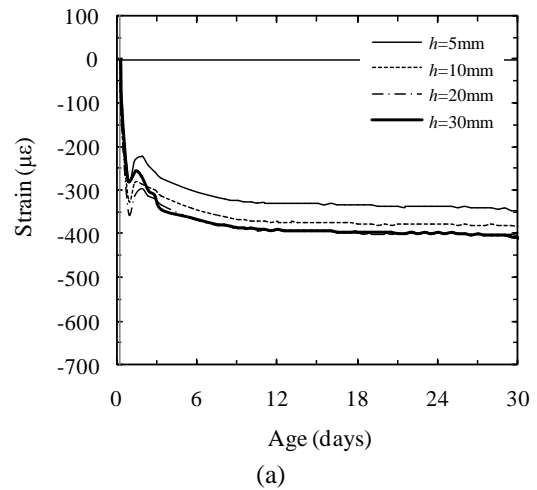


Fig. 8 Comparison of strains in steel rebar and concrete

in the steel rebar and the concrete near the steel rebar. These restrained strains showed similar behavior each other. However, the strain measured in the steel rebar varied with temperature because steel is relatively more sensitive to temperature gradient than concrete. Thus, in this study, the restrained strains measured in concrete near the steel rebar were used as restrained strains to minimize the instability of data due to the temperature gradient. Owing to restraint of concrete shrinkage from the steel rebar, the restrained strains were much lower than the shrinkage strain of concrete without rebar. For example, the 30-day restrained strain for $d_b=15.9$ mm was found to be $-187 \mu\epsilon$, which is about 69% lower than the shrinkage strain of concrete without rebar measured at the same depth.

Fig. 9 shows the restrained strain behavior in terms of the diameter of the upper steel rebar and the cover depth. For all test series, the rebar was slightly expanded at an early age owing to the hydration heat of concrete and the inclusion of EA. The restrained strain decreased with increasing rebar diameter. The decrease in the restrained strain with increasing rebar diameter, leading to increasing reinforcement ratio, was obtained, and it was mostly observed at a very early age before the slight expansion. This is caused by the following reasons. To deform the steel

Fig. 9 Restrained strain behaviors; (a) $d_b=9.5$ mm, (b) $d_b=15.9$ mm, (c) $d_b=22.2$ mm

rebar with a larger diameter, a higher compressive force is required as compared to that with a smaller diameter. However, the dimension of tested slabs was identical to be $600 \times 600 \times 100$ mm, so that the force applied by shrinkage of UHPFRC could simply be assumed to be also identical. Consequently, smaller restrained strain was generated with larger steel rebars, because of the decreased stress by the shrinkage compressing the steel rebars. In addition, no

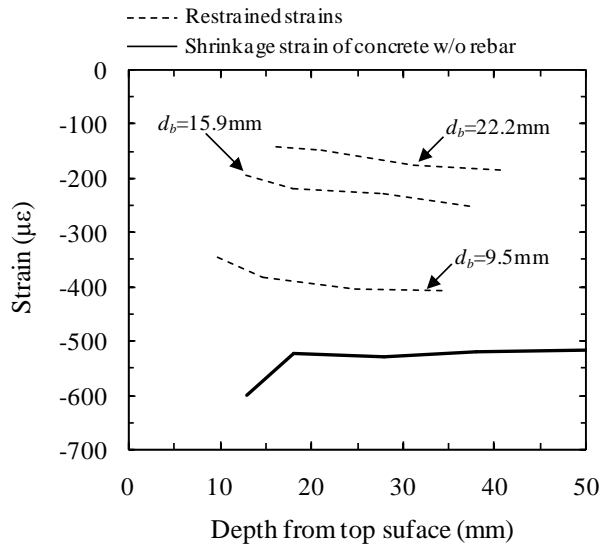


Fig. 10 Comparison of restrained strains and shrinkage strain of concrete without rebar after 30 days

shrinkage cracking, caused by the restraint of shrinkage from the steel rebar, was observed until 30 days because of the superior tensile strength development of UHPFRC.

Comparison of the restrained strains and the shrinkage strain of concrete without rebar after 30 days is illustrated in Fig. 10. Regardless of the rebar diameter, all test specimens showed an increase in the restrained strain with increasing cover depth. This is attributed to the fact that a smaller cover depth was insufficient to transfer the full restraint force from the concrete to the steel rebar. In addition, smaller cover depth decreased the effective volume of concrete forcing to deform the steel rebar, so that lower restrained strains were obtained. This is consistent with the findings from a previous study (Yoo *et al.* 2014b) reporting that a smaller restrained strain of steel rebar was obtained when a larger reinforcement ratio, which indicates a smaller effective volume of concrete, was applied. Higher restrained strain was also observed at a smaller rebar diameter, because a lower steel rebar diameter resulted in higher compressive stress at the identical compressive force by shrinkage. A similar observation that the restrained strain in steel rebar increases with decreasing the rebar diameter has been reported in a previous study (Chen and Choi 2011).

3.3 Degree of restraint

If the shrinkage of concrete is perfectly restrained by steel rebars, the measured strain in the steel rebar should be equal to zero. However, in general, reinforcing steel is deformed by concrete shrinkage, as shown in Fig. 9, so that the restraint strain according to inner steel rebar can be defined as the difference between the strains in the concrete without rebar and the steel rebar, as follows

$$\varepsilon_r = \varepsilon_{sh} - \varepsilon_s \quad (1)$$

where ε_{sh} is the shrinkage strain of concrete without rebar, ε_s is the strain in the steel rebar, and ε_r is the restraint strain.

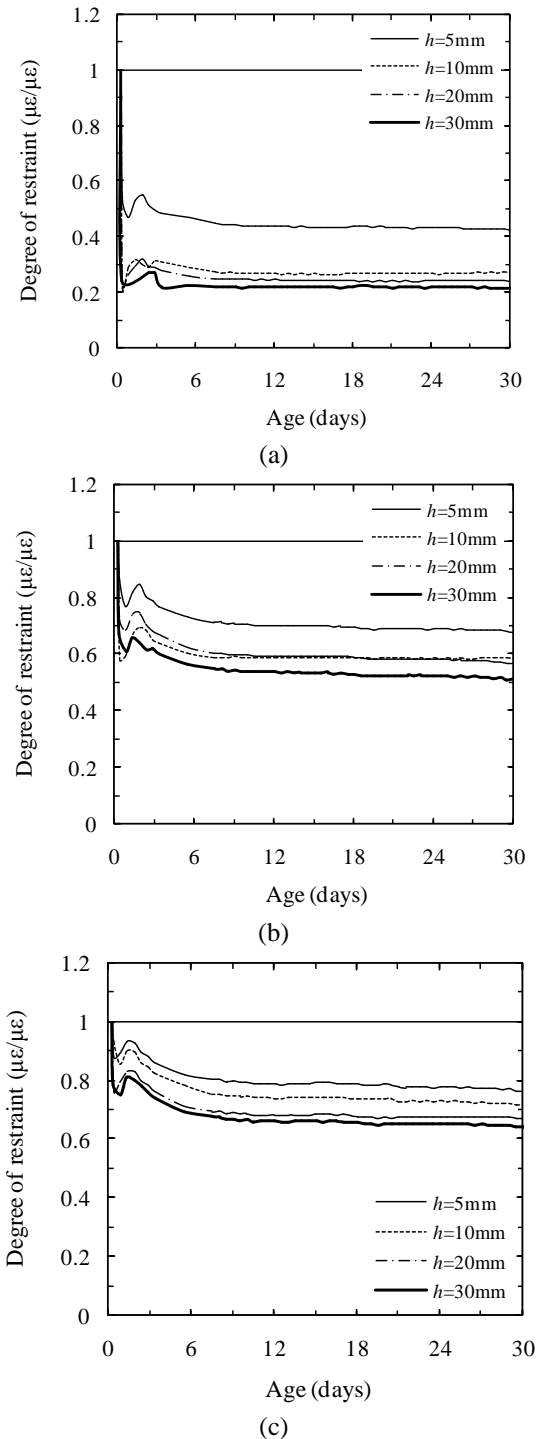


Fig. 11 Degree of restraint; (a) $d_b=9.5$ mm, (b) $d_b=15.9$ mm, (c) $d_b=22.2$ mm

The degree of restraint, ψ , is thus defined as the ratio between the restraint strain and the shrinkage of concrete without rebar, as expressed by Eq. (2) below

$$\psi = \frac{\varepsilon_r}{\varepsilon_{sh}} = 1 - \frac{\varepsilon_s}{\varepsilon_{sh}} \quad (2)$$

Figs. 11 and 12 exhibit the calculated degree of restraint with various rebar diameters and cover depths. As reported by Yoo *et al.* (2014b), a higher reinforcement ratio (in this

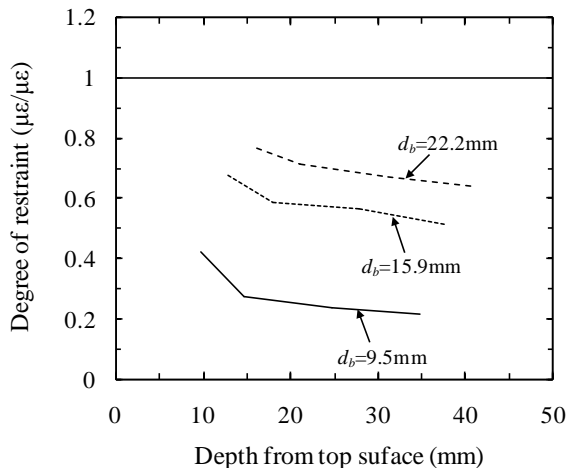


Fig. 12 30-day degree of restraint according to rebar diameter and cover depth

study, a higher rebar diameter) resulted in a higher degree of restraint. This is because lower strain in the steel rebar was observed for the specimens with a higher rebar diameter (see Fig. 9). For example, the degree of restraint for the specimen with $d_b=9.5$ mm and $h=30$ mm was found to be 0.22 after 30 days: this value is approximately 58% and 66% lower than those for the specimens with $d_b=15.9$ mm and $d_b=22.2$ mm at $h=30$ mm, respectively. For all test series, the degree of restraint was reduced with increasing cover depth. This is because the effective volume of concrete forcing steel rebar to be reduced was increased, and similar to the findings from Yoo *et al.* (2017) that the degree of restraint decreased with increasing the thickness of concrete relative to the thickness of restraint steel. In addition, the degree of restraint decreased with time because of the increases in the free shrinkage and elastic modulus of concrete. From these observations, it can be concluded that the use of steel rebar with a higher diameter and a lower cover depth is unfavorable as it deteriorates the restrained shrinkage performance of UHPFRC: a higher degree of restraint normally leads to higher residual stress and cracking potential in concrete (Hossain and Weiss 2004). However, to quantitatively evaluate the residual stress generated in concrete by restraint of shrinkage, additional study on numerical simulation is required to be done.

4. Conclusions

In this study, the restrained shrinkage behavior of UHPFRC slabs was investigated. For this, twelve large-sized UHPFRC slabs with various rebar diameters and cover depths were fabricated. In addition, to evaluate degree of restraint, a same-sized UHPFRC slab without steel rebar was fabricated.

The zeroing point of shrinkage measurement was determined as the start time of stress development in concrete due to restraint of shrinkage. Shrinkage strains steeply increased from the zeroing point up to 16 h and then the specimen slightly expanded. After the slight expansion,

the strains gradually increased and converged to a stable value. The shrinkage strain near the exposed surface was high because of water evaporation. However, below a depth of 18 mm, the shrinkage strains were seldom influenced by the depth and showed a similar value.

The strains measured in the steel rebar were much lower than the shrinkage strains of concrete without rebar due to the restraint of shrinkage from the steel rebar. The restrained strain decreased with increasing rebar diameter, leading to an increase of reinforcement ratio, and with decreasing cover depth, and a great part of the decrease in the restrained strain was observed at a very early age. Owing to the superior tensile strength of UHPFRC, no shrinkage cracking was observed until 30 days. The steel rebar with a larger diameter and a lower cover depth showed a higher degree of restraint. Since a higher degree of restraint generally results in higher residual stress and cracking potential, it was concluded that the use of steel rebar with a large diameter, causing a larger reinforcement ratio, and the application of a low cover depth are unfavorable regarding the restrained shrinkage performance of UHPFRC slabs.

Acknowledgements

This work was supported by the National Research Foundation of Korea (NRF) grant funded by the Korea government (MEST) (NRF-2016R1A2B3011392).

References

- AFGC (2013), Ultra high performance fibre-reinforced concretes. Interim Recommendations, AFGC Publication, France.
- Aitcin, P.C. (1999), "Demystifying autogenous shrinkage", *Concrete Int.* **21**(11), 54-56.
- American Society for Testing and Materials (ASTM) (2007), ASTM C 1437 Standard test method for flow of hydraulic cement mortar, Annual book of ASTM standards, ASTM, West Conshohocken, PA.
- American Society for Testing and Materials (ASTM) (2008), ASTM C 403 Standard test method for time of setting of concrete mixture by penetration resistance, Annual book of ASTM standards, ASTM, West Conshohocken, PA.
- American Society for Testing and Materials (ASTM) (2008), ASTM C 157/C 157M Standard test method for length change of hardened hydraulic-cement mortar and concrete, Annual book of ASTM standards, ASTM, West Conshohocken, PA.
- Chang-Wen, M., Qian, T., Wei, S. and Jia-Ping, L. (2007), "Water consumption of the early-age paste and the determination of "time-zero" of self-desiccation shrinkage", *Cement Concrete Res.*, **37**(11), 1496-1501.
- Chen, H.L.R. and Choi, J.H. (2011), "Analysis of shrinkage and thermal stresses in concrete slabs reinforced with GFRP rebars", *J. Mater. Civil Eng.*, **23**(5), 612-627.
- Graybeal, B.A. (2008), "Flexural behavior of an ultrahigh-performance concrete I-girder", *J. Bridge Eng.*, **13**(6), 602-610.
- Habel, K., Charron, J.P., Denarie, E. and Bruhwiler, E. (2006), "Autogenous deformations and viscoelasticity of UHPFRC in structures. Part 1: Experimental results", *Mag. Concr. Res.*, **58**(3), 135-145.
- Hossain, A.B. and Weiss, W.J. (2004), "Assessing residual stress development and stress relaxation in restrained concrete ring

- specimens”, *Cement Concrete Compos.*, **26**(5), 531-540.
- Japan Concrete Institute (JCI) (1999), Committee report, In: Tazawa E, editor, *Autogenous shrinkage of concrete*, E&FN Spon.
- Japan Society of Civil Engineers (JSCE) (2004), Recommendations for design and construction of ultra-high strength fiber reinforced concrete structures (Draft), Japan Society of Civil Engineers, Tokyo, Japan.
- Jiang, C., Yang, Y., Wang, Y., Zhou, Y. and Ma, C. (2014), “Autogenous shrinkage of high performance concrete containing mineral admixtures under different curing temperatures”, *Constr. Build. Mater.*, **61**, 260-269.
- Kamen, A., Denarié, E. and Brühwiler, E. (2007), “Thermal effects on physico-mechanical properties of ultra-high-performance fiber-reinforced concrete”, *ACI Mater. J.*, **104**(4), 415-423.
- Kim, Y.J., Park, S.Y., Park, J.S. and Kim, B.S. (2013), “State-of-the-art of UHPC applications in the World”, *Korean Soc. of Civil Eng.*, **61**(2), 39-50. (in Korean)
- Kobler, M. and Sobek, W. (2008), “The introduction of high forces into thin-walled UHPC elements by the use of implants”, *Proceedings of the Second International Symposium on Ultra High Performance Concrete*, Kassel, Germany, 683-690.
- Park, J.J., Yoo, D.Y., Kim, S.W. and Yoon, Y.S. (2013), “Drying shrinkage cracking characteristics of ultra-high-performance fibre reinforced concrete with expansive and shrinkage reducing agents”, *Mag. Concrete Res.*, **65**(4), 248-256.
- Park, J.J., Yoo, D.Y., Kim, S.W. and Yoon, Y.S. (2014), “Benefits of using expansive and shrinkage reducing agents in ultra-high-performance concrete for volume stability”, *Mag. Concrete Res.*, **66**(14), 745-750.
- Perry, V. and Weiss, G. (2009), “Innovative field cast UHPC joints for precast bridge decks-Design, prototype testing and projects”, *Proceedings of the International Workshop on Ultra High Performance Fibre Reinforced Concrete*, Designing and Building with UHPFRC: State of the Art Development, Marseille, France, AFGC/fib.
- Rajabipour, F., Sant, G. and Weiss, J. (2008), “Interactions between shrinkage reducing admixtures (SRA) and cement paste’s pore solution”, *Cement Concrete Res.*, **38**(5), 606-615.
- Richard, P. and Cheyrezy, M. (1995), “Composition of reactive powder concretes”, *Cement Concrete Res.*, **25**(7), 1501-1511.
- Saleem, M.A., Mirmiran, A., Xia, J. and Mackie, K. (2011), “Ultra-high-performance concrete bridge deck reinforced with high-strength steel”, *ACI Struct. J.*, **108**(5), 601-609.
- Sant, G., Lothenbach, B., Juilland, P., Le Saout, G., Weiss, J. and Scrivener, K. (2011), “The origin of early age expansions induced in cementitious materials containing shrinkage reducing admixtures”, *Cement Concrete Res.*, **41**(3), 218-229.
- Yoo, D.Y., Banthia, N. and Yoon, Y.S. (2015), “Effectiveness of shrinkage-reducing admixture in reducing autogenous shrinkage stress of ultra-high-performance fiber-reinforced concrete”, *Cement Concrete Compos.*, **64**, 27-36.
- Yoo, D.Y., Park, J.J., Kim, S.W. and Yoon, Y.S. (2013), “Early age setting, shrinkage and tensile characteristics of ultra high performance fiber reinforced concrete”, *Const. Build. Mater.*, **41**, 427-438.
- Yoo, D.Y., Park, J.J., Kim, S.W. and Yoon, Y.S. (2014b), Influence of reinforcing bar type on autogenous shrinkage stress and bond behavior of ultra high performance fiber reinforced concrete,” *Cement Concrete Compos.*, **48**, 150-161.
- Yoo, D.Y., Park, J.J., Kim, S.W. and Yoon, Y.S. (2014c), “Combined effect of expansive and shrinkage-reducing admixtures on the properties of ultra high performance fiber-reinforced concrete”, *J. Compos. Mater.*, **48**(16), 1981-1991.
- Yoo, D.Y., Shin, H.O., Yang, J.M. and Yoon, Y.S. (2014a), “Material and bond properties of ultra high performance fiber reinforced concrete with micro steel fibers”, *Compos. Part B-Eng.*, **58**, 122-133.
- Yoo, D.Y., Yoon, Y.S. and Banthia, N. (2017), “Ultra-high-performance fiber-reinforced concrete: Shrinkage strain development at early ages and potential for cracking”, *J. Test. Eval.*, doi: <http://dx.doi.org/10.1520/JTE20160114>. (in Press)

CC